ORIGINAL RESEARCH

Folic Acid Decorated Zeolitic Imidazolate Framework (ZIF-8) Loaded with Baicalin as a Nano-Drug Delivery System for Breast Cancer Therapy

Xiao Mi[1]
Meigeng Hu[1]
Mingran Dong[1]
Zhihong Yang[1]
Xia Zhan[2]
Xinyue Chang[1]
Juan Lu[1]
Xi Chen[1]

[1]Institute of Medicinal Plant Development, Chinese Academy of Medical Sciences, Peking Union Medical College, Beijing, 100094, People's Republic of China; [2]Key Laboratory of Cleaner Production and Integrated Resource Utilization of China National Light Industry, Beijing Technology and Business University, Beijing, 100048, People's Republic of China

Correspondence: Xi Chen; Juan Lu
Institute of Medicinal Plant Development, Chinese Academy of Medical Sciences, Peking Union Medical College, Beijing, 100094, People's Republic of China
Tel +86 10-57833257
Email chenxi@implad.ac.cn;
jlu@implad.ac.cn

Background: Baicalin (BAN) has attracted widespread attention due to its low-toxicity and efficient antitumor activity, but its poor water solubility and low bioavailability severely limit its clinical application. Development of a targeted drug delivery system is a good strategy to improve the antitumor activity of baicalin.

Methods: We prepared a BAN nano-drug delivery system PEG-FA@ZIF-8@BAN with a zeolite imidazole framework-8 (ZIF-8) as a carrier, which can achieve the response of folate receptor (FR). We characterized this system in terms of morphology, particle size, zeta-potential, infrared (IR), ultraviolet (UV), x-ray diffraction (XRD), and Brunel-Emmett-Teller (BET), and examined the in vitro cytotoxicity and cellular uptake properties of PEG-FA@ZIF-8@BAN using MCF-7 cells. Lastly, we established a 4T1 tumor-bearing mouse model and evaluated its in vivo anti-mammary cancer activity.

Results: The PEG-FA@ZIF-8@BAN nano-delivery system had good dispersion with a BAN loading efficiency of $41.45 \pm 1.43\%$, hydrated particle size of 176 ± 8.1 nm, Zeta-potential of -23.83 ± 1.1 mV, and slow and massive drug release in an acidic environment (pH 5.0), whereas release was 11.03% in a neutral environment (pH 7.4). In vitro studies showed that PEG-FA@ZIF-8@BAN could significantly enhance the killing effect of BAN on MCF-7 cells, and the folic acid-mediated targeting could lead to better uptake of nanoparticles by tumor cells and thus better killing of cancer cells. In vivo studies also showed that PEG-FA@ZIF-8@BAN significantly increased the inhibition of the proliferation of solid breast cancer tumors ($p < 0.01$ or $p < 0.001$).

Conclusion: The PEG-FA@ZIF-8@BAN nano-drug delivery system significantly enhanced the anti-breast cancer effect of baicalin both in vivo and in vitro, providing a more promising drug delivery system for the clinical applications and tumor management.

Keywords: metal-organic framework, folic acid response, baicalin, breast cancer therapy

Introduction

Breast cancer, one of the most common cancers in women, is characterized by high morbidity, poor prognosis, and limited treatment options. Chemotherapy for breast cancer is usually administered in the form of a single antitumor agent, and side effects and drug resistance are major challenges.[1] Moreover, the high cost of most clinical anti-cancer drugs places a significant financial burden on patients and their families.[2] There is an urgent need for novel antitumor treatment options that have less toxicity, are more resistant to drug resistance, and are more affordable.[3,4]

Targeted nano drug delivery systems have shown advantages over conventional drug treatment modalities due to their ability to enhance drug aggregation at the tumor site and specific drug delivery modalities. However, most of the drug carriers currently used suffer from inadequate long-term safety, poor biocompatibility, high manufacturing costs, and limited drug delivery efficiency,[5] hence, developing stable drug delivery systems with targeted anticancer effects with low toxicity and good biocompatibility is key to improving the effectiveness of breast cancer treatment.

BAN is one of the main active ingredients in Scutellaria baicalensis Georgi, family Labiatae, with pharmacological effects such as antibacterial, anti-inflammatory, antihypertensive, and anti-allergic.[6,7] The literature reports the prominent antitumor activity of BAN against a variety of tumor types, such as colon cancer,[8,9] liver cancer,[10] bladder cancer[11] and glioblastomas.[12] The anti-tumor effects are mainly reflected in inducing apoptosis, cell cycle arrest, and autophagy, and inhibiting angiogenesis and metastasis.[13,14] Studies have shown that BAN could induce tumor cell apoptosis through a variety of pathways.[15] BAN could induce apoptosis and suppress migration/invasion of MDA-MB-231 cells via ROS-mediated activation of the p38/JNK signaling pathway.[16] It also confirmed that BAN-induced apoptotic cell death in breast cancer cells involves the up-regulation of proapoptotic p53 and bax.[17] However, the presence of sugar groups in the molecular structure of BAN leads to its low hydrophilicity (solubility 0.052 mg/mL in water) and lipophilicity (Papp = 0.037×10^{-6} cm/s),[18] and its bioavailability after oral administration is only 2.2%,[19] all of which limit its clinical application. However, the preparation of BAN into novel nano formulations can modify its physical properties and improve its bioavailability.

Metal-organic frameworks (MOFs) have high surface area, high porosity, tunable pore structure, and easy surface functionalization. They have great potential for applications in such areas as biosensing, bioimaging, and drug delivery.[20,21] In recent years, zeolite imidazole framework-8 (ZIF-8) has received much attention as an emerging class of nano metal-organic frameworks (NMOFs). ZIF-8 is characterized by a simple synthetic strategy, easy functionalization, high loading capacity, and pH-responsive degradation.[22] Due to these characteristics, nanoparticles of ZIF-8 have been widely used for DNA, protein, and drug delivery.[23–26] Therefore, the potential of ZIF-8-based nano drug delivery systems for hydrophobic drug-targeted intracellular delivery is worth exploring.

Folate is one of the most widely used small molecules in the study of targeted drug delivery systems and has an important role in the synthesis of DNA and RNA.[27] In normal tissue cells, folate enters the cell by transmembrane, while in cancer cells, folate receptors on the cell surface recognize folate and form folate complexes, at which point endocytic vesicles are formed to enter the cancer cell by internalization, which is the main way that folate molecules recognize and enter cancer cells.[28,29] Based on the fact that folate enters normal cells and tumor cells in different ways, it can be modified to the carrier surface as a targeting molecule, so that the drug delivery system can selectively enter tumor cells and release the loaded drug in the cytoplasm to play the role of anti-cancer agent in biomedicine and achieve targeted therapy for tumors.[30] The current research on folic acid focuses on folic acid polymer targeted drug delivery systems, such as the folic acid polyethylene glycol drug delivery system,[31,32] folic acid amphiphilic block copolymers[33,34] and so on. Many reports have shown that folic acid modified nanoparticles can target many kinds of cancer cells including breast cancer cells.[35–37] Human breast cancer cell MCF-7, as a FR overexpression cell line, has been used to evaluate various folate targeted nanoscale platforms.[38–41]

Based on the idea suggested, we prepared a BAN nano delivery system using ZIF-8 as a carrier and Polyethylene glycol–folate (PEG-FA) as a target modification group. ZIF-8 was synthesized by coordination of 2-methylimidazole with Zn^{2+}(molar ratio 4:1) and loaded with BAN by stirring at room temperature, followed by PEG-FA targeting modification on its surface to obtain PEG-FA@ZIF-8@BAN. Then the morphology, particle size, zeta-potential, IR, UV, XRD, and BET were characterized, and the release characteristics were investigated. In vitro cytotoxicity and cellular uptake studies of PEG-FA@ZIF-8@BAN were performed using MCF-7 cells, and their biocompatibility was evaluated. Finally, 4T1 tumor-bearing mouse model was established to study the in vivo anti-breast cancer activity of PEG-FA@ZIF-8@BAN. The nano drug delivery system can realize the response of folate receptor to increase the anti-tumor effect of the drug, which has a good development prospect.

Materials and Methods
Reagents and Instrument
Zinc nitrate hexahydrate (Zn $(NO_3)_2 \cdot 6H_2O$,99%) was purchased from Tianjin FuChen Chemical Reagent Co., Ltd, China. 2-methylimidazole ($C_4H_6N_2$,98%) was obtained from TCI Development Co., Ltd, China. BAN was

purchased from Shanghai Winherb Medical Technology Co., Ltd,China. mPEG-FA was purchased from Shanghai Ponsure Biotechnology Co., Ltd, China. Fetal bovine serum was obtained from PAN Seratech GmbH, Germany. Anti-folate primary mouse monoclonal antibody (sc-515521) was purchased from Santa Cruz Biotechnology, Inc (Dallas, Texas). Goat Anti-Mouse secondary antibody conjugated to Alexa Fluor 488 was purchased from Shanghai Beyotime Biotechnology Co., Ltd, China. The absorbance was detected by TECAN spark multifunctional microplate reader. Cell Counting Kit-8 (CCK-8) was purchased from Dojindo Laboratories (Kumamoto, Japan). Fluorescence images were taken using a Nikon Eclipse Ts2R fluorescence inverted microscope. Confocal laser scanning microscopy (CLSM) images were taken on Leica SP8. The loading efficiency and release rate were measured by Agilent Technologies Cary series UV-vis spectrophotometer. The blood biochemical indexes of the mice were detected by a Beckman Kurt AU480 automatic biochemical analyzer.

Cell Lines and Animals

Human breast cancer cell line MCF-7 cells and mouse epithelioid fibroblast L929 cells were purchased from the Cell Resource Center, Institute of Basic Medical Sciences, Chinese Academy of Medical Sciences. All cells were cultured at 37°C in 5% CO_2.

Healthy 20–22g BALB/c mice were provided by SBF (Beijing) experimental animal Technology Co., Ltd. All animals were housed in a facility with a barrier system under the conditions as follows: temperature, 17–25°C, humidity, 45–80%, and 12 hours light/dark cycle. All procedures were approved by the research animal ethics committee of the Institute of Medicinal Plant Development affiliated to the Chinese Academy of Medical Sciences (Beijing, China, Ethical review No. SLXD-20210621019). 2.5–3 kg New Zealand white rabbits were purchased from Beijing Fang Yuan farm and fed normally in the rabbit laboratory. All the animal experiments were conducted in accordance with the National Institutes of Health Guide for Care and Use of Laboratory Animals.

Synthesis of PEG-FA@ZIF-8@BAN

Synthesis of ZIF-8: 2.975 g of zinc nitrate hexahydrate and 3.284 g of 2-methylimidazole (molar ratio 1:4) were weighed precisely, dissolved in methanol, and stirred at 1000 rpm for 1.5 hours, and after standing for 24 hours, the precipitate was collected by centrifugation at 8000 rpm

for 10 minutes, and then washed three times with methanol and dried under vacuum at 60°C to obtain ZIF-8.

Synthesis of ZIF-8@BAN: ZIF-8 was re-dispersed in methanol by ice bath sonication for 20 minutes, and then a certain amount of BAN was sonicated and dissolved in methanol; the two solutions were mixed and stirred at 600 rpm at room temperature for 12 hours. The precipitate was collected by centrifugation at 8000 rpm for 10 minutes, and then the methanol was washed three times and ZIF-8@BAN was obtained by vacuum drying at 60°C. The optimal loading ratio was investigated by controlling the feeding amount of BAN.

Synthesis of PEG-FA@ ZIF-8@BAN: 50 mg of PEG-FA was dissolved in 5 mL of deionized water solution; 50 mg of ZIF-8@BAN was added and stirred for 48 hours at room temperature and protected from light, and the resulting precipitate was washed three times with deionized water and centrifuged at 11,000 rpm. The resulting solid was dried under vacuum to obtain PEG-FA@ZIF-8@BAN.

Characterization of Nanoparticles

Transmission Electron Microscopy (TEM) micrographs were obtained from a FEI Talos F200X transmission electron microscope. Scanning electron microscopy (SEM) images were obtained using a ZEISS Sigma 500 scanning electron microscope. Size and zeta potential measurements of ZIF-8, ZIF-8@BAN and PEG-FA@ZIF-8@BAN were measured by Malvern Zetasizer Nano ZS90. Each nanoparticle system was measured three times. XRD were recorded on a Rigaku Smartlab SE diffractometer. The UV–vis absorption spectra were determined by a PE-Lambda 950 spectro photometer. FT-IR was collected on a Thermo Scientific Nicolet iN10 spectro photometer using KBr pellets. Nitrogen adsorption/desorption analysis was obtained from Micromeritics ASAP 2460.

Determination of Drug Loading and Drug Release

The drug loading efficiency (DLE%) and entrapment efficiency (EE%) was measured by UV spectrophotometer at 278 nm absorption wavelength, and the standard curve of the BAN solution was established in the concentration range of 5–40 μg/mL. The DLE% and EE% were calculated using the following equations:

$$DLE(\%) = \frac{W_1}{W_t} \times 100\%$$

$$EE(\%) = \frac{W_1}{W_0} \times 100\%$$

Where: W_0 is the weight of the total drug added, W_1 is the weight of the drug loaded in the nanoparticles and W_t is the total weight of the nanoparticles.

The in vitro release rate of the drug was also measured using a UV spectrophotometer. The dynamic membrane dialysis method was used to investigate the in vitro release characteristics of the nanosystem. ZIF-8@BAN and PEG-FA@ZIF-8@BAN were dispersed in phosphate-buffered saline (PBS) buffer solutions of different pH (7.4 and 5.0), and then placed in the processed dialysis bag (molecular weight cut off 3500 Da). The dialysis bag was placed in a release tube containing 10 mL of PBS with the corresponding pH, and then the tubes were placed in a water bath shaker at 37°C and gently shaken at 100 r/min; 0.5 mL of supernatant was removed at the specified time and supplemented with an equal volume of fresh PBS, diluted at appropriate multiples and assayed in the absorbance range, and finally, the cumulative release rate of the drug was calculated. The Korsmeyer-Peppas model was used to fit the drug release curve.

Immunofluorescence for FR Expression

Cells were seeded in a 6-well chamber slide at a density of 5×10^5 cells/mL, 2 mL/well. After overnight incubation in a humidified chamber at 37°C, cells were washed with ice-cold $1 \times$ PBS and fixed with 4% paraformaldehyde for 20 min at room temperature. After removing paraformaldehyde, the cells were washed three times with $1 \times$ PBS for 3 min each, and blocked for 30 min with $1 \times$ PBS containing 10% goat serum. Cells were then incubated 2 h with mouse monoclonal anti-FR antibody at 37°C. After incubation, cells were washed repeatedly with $1 \times$ PBS (3 times, 3 min each) and incubated with the fluorochrome-conjugated secondary antibody for 30 min at room temperature. Cells were washed three times in $1 \times$ PBS and incubated with 0.5 μg/mL DAPI for 5 min. Cell fluorescence images were taken using a fluorescent inverted microscope.

Cytotoxicity Assay

MCF-7 cells were inoculated in 96-well plates at a density of about 6×10^3 per well, and then incubated in a constant-temperature cell culture incubator at 37°C for 24 hours. The culture medium was removed and re-added with BAN, ZIF-8@BAN, PEG-FA@ZIF-8@BAN cell culture

medium containing the same BAN concentration to continue incubation for 12 hours or 24 hours. The control group was incubated with culture medium only. After incubation, the medium was aspirated and discarded; 100 μL of Cell Counting Kit-8 (CCK-8) dilution solution was added, and the absorbance value of each well was measured at 450 nm using an enzyme marker at the end of 1 hour incubation in the incubator. To examine the in vitro compatibility of the nanomaterials, a blank PEG-FA@ZIF-8 group was set up and the toxic effects of the blank material on the cells were examined using the cancer cell line MCF-7 and the normal cell line L929 cells. Cell viability was calculated according to the formula:

$$cell\ viability(\%) = \frac{A_s - A_b}{A_c - A_b} \times 100\%$$

where A_s is the experimental well, A_c is the control well, and A_b is the blank well.

Live and Dead Cell Staining

MCF-7 cells were inoculated in 12-well culture dishes at a concentration of 5×10^4 cells per well and cultured for 24 hours. After cell apposition, fresh media containing BAN, ZIF-8@BAN, and PEG-FA@ZIF-8@BAN were replaced with 40 μg/mL of BAN in each group. Cells were treated with blank nanomaterials containing the same amount of PEG-FA@ZIF-8 to examine the biocompatibility of the material, and cells treated with PEG-FA preincubation for 2 hours were continued to examine PEG-FA@ ZIF-8@BAN bio targeting. After the interaction with the drug, the residual drug was washed off with PBS and 0.5 mL Calcein – AM/PI solution was added to stain the cells for 30 minutes, and cell fluorescence images were taken using a fluorescent inverted microscope. In the control group, no drug was added.

Cellular Uptake Experiments

MCF-7 cells were used to examine the cellular uptake behavior of PEG-FA@ZIF-8@BAN. Approximately 1×10^5 MCF-7 cells were inoculated in 6-well culture plates and incubated for 24 hours in a cell culture incubator after apposition. ZIF-8@BAN, PEG-FA@ZIF-8@BAN solution, and PEG-FA@ZIF-8@BAN were added to cells pre-incubated with free PEG-FA, followed by incubation for 0.5 hour or 3 hours. At the set time point, the cells were washed several times with PBS to remove the residual nanomaterials. After fixation with 4% paraformaldehyde, Hoechst 33342 dye for staining the

nuclei and 2,7-dichloro-dihydro-fluorescein diacetate (DCFH-DA) for measuring intracellular reactive oxygen species (ROS) production were added for observation under a laser scanning confocal microscope.

Hemolytic Test

Blood was extracted by puncturing the hearts of New Zealand rabbits, and 2% erythrocyte suspension was prepared by stirring with a glass rod to remove fibrin. 2% erythrocyte suspension, PBS, and test solution were added, as specified, using PBS as a negative and purified water as a positive control, mixed well, and immediately placed in a constant temperature water bath at 37°C ± 0.5°C for warming. The hemolysis and coagulation reactions were observed after 3 hours, and the absorbance was measured at 414 nm using an enzyme marker.

In vivo Experiments

In vivo experiments were performed using 4T1 inoculated female BALB/c mice. 4T1 cells were dispersed in physiological saline at a density of 1×10^6 cells/mL, and 0.2 mL of cell suspension was subcutaneously inoculated into the axilla of the right forelimb of mice to establish a mouse breast cancer model. When the tumor-bearing mice reached a tumor volume of approximately 100 mm^3, they were randomly divided into 4 groups of 7 mice per group. Each group of mice was injected with PBS, BAN, ZIF-8@BAN, PEG-FA@ZIF-8@BAN solution in tail vein every two days for 15 days, and the tumor volume was measured every two days, and the tumor volume was $V = L \times W^2/2$ (where L and W refer to the longest and shortest diameter of the tumor, respectively). The relative tumor volume was V/V_0 (V_0 was the initial tumor size of the mice carrying the tumor). After in vivo drug efficacy experiments were completed, blood was removed from the eyes of the mice and serum was collected for determination of blood biochemical parameters. The mice were dissected and weighed, and the tumors and major organs (heart, liver, spleen, lungs, and kidneys) were collected, followed by hematoxylin and eosin stain (H&E) and terminal deoxynucleotide transfer modification dUTP-biotin end-labeling (TUNEL) staining tests.

Statistics

Data are expressed as mean ± SD. Statistical evaluation was performed by two-tailed Student's t-test or one-way ANOVA. ns represents no statistical significance, * is $p < 0.05$, ** is $p < 0.01$, and *** is $p < 0.001$.

Results and Discussion
Synthesis and Characterization of Nanoparticles

Scheme 1 demonstrates a simple synthetic strategy for the PEG-FA@ZIF-8@BAN nano delivery system and its application in cancer therapy. 2-methylimidazole and Zn^{2+} formed ZIF-8 by coordination, and then BAN was loaded into the high porosity ZIF-8 carrier by ambient stirring method, and finally PEG-FA was modified on the surface of the drug delivery system to achieve tumor targeting. When administered intravenously, PEG-FA ensures that the nano delivery system is not degraded under normal physiological conditions and is intelligently targeted for rapid enrichment in tumor cells with high expression of the folate receptor. By degrading the outer layer of PEG-FA in the acidic environment of reduced pH in cancer cells, the ligand bond of ZIF-8 is also gradually broken in the acidic environment, thus releasing the drug slowly. Thus far, we have successfully constructed a tumor-specific response drug delivery system.

The materials were synthesized and morphologically observed by scanning electron microscopy (SEM) and transmission electron microscopy (TEM). As can be seen in Figures 1Aa–c and S1, the SEM images of ZIF-8, ZIF-8@BAN, PEG-FA@ZIF-8@BAN show that the average diameters of the synthesized uniformly dispersed nanoparticles are 89.53 nm, 90.85 nm, and 96.52 nm, respectively. As shown in TEM image Figure 1Ad–f, the synthesized ZIF-8 material has a rhombic dodecahedral three-dimensional structure with sharp edges that is consistent with the literature. Compared with the obvious stereoscopic structure of ZIF-8, the morphology of ZIF-8@BAN and PEG-FA@ZIF-8@BAN gradually become less regular and the angles become blurred, indicating the successful loading and surface modification of the guest molecule by ZIF-8.

The hydrated particle sizes of ZIF-8, ZIF-8@BAN and PEG-FA@ZIF-8@BAN were determined by a Malvern Mastersizer. As shown in Figure 1Ba–c, the particle size measurements were 155 ± 2.9 nm, 161.13 ± 1.19 nm and 176 ± 8.1 nm, respectively. Each had a narrow size distribution and good water dispersion. The size of PEG-FA@ZIF-8@BAN was significantly larger than that of ZIF-8, which could prove the successful loading of the drug and modification of PEG-FA. The hydrodynamic particle size of the nanoparticles measured by DLS was slightly larger than that observed by SEM, which may be caused by the
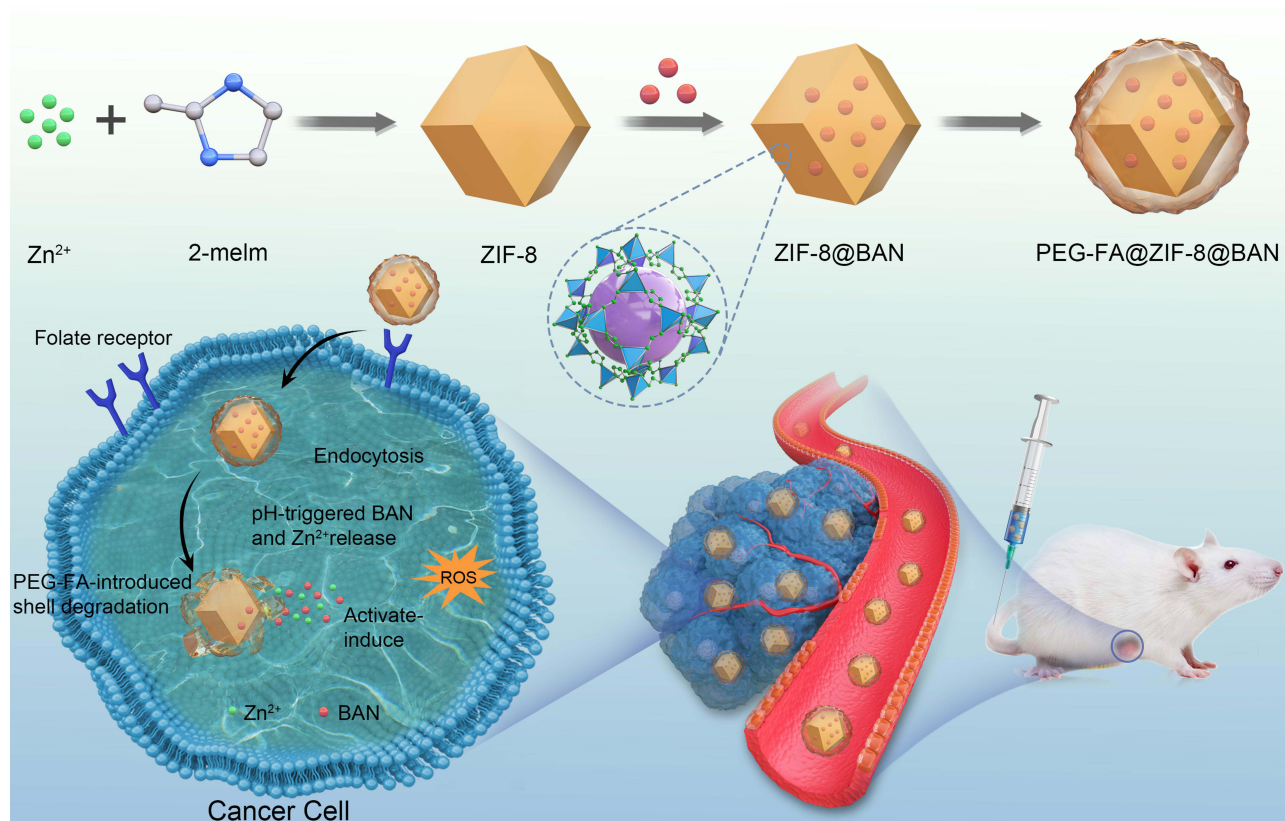
Scheme 1 PEG-FA@ZIF-8@BAN schematic representation of the formation of a nano platform. Schematic diagram of effective antitumor therapy with responsive drug delivery system mediated by folate receptor.
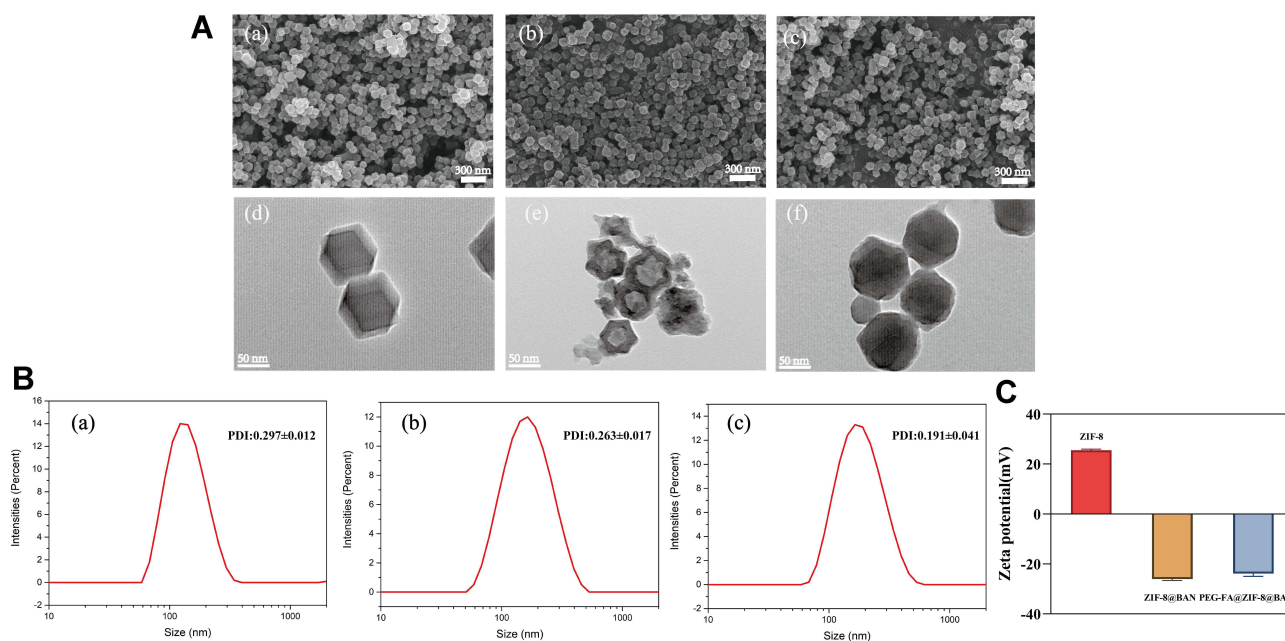

Figure 1 (**A**) SEM images of ZIF-8 (a, 300 nm), ZIF-8@BAN (b, 300 nm), and PEG-FA@ZIF-8@BAN (c, 300 nm) and TEM images of ZIF-8 (d, 50 nm), ZIF-8@BAN (e, 50 nm), and PEG-FA@ZIF-8@BAN (f, 50 nm). (**B**) Size distribution of DLS measured by ZIF-8 (a), ZIF-8@BAN (b), and PEG-FA@ZIF-8@BAN (c) (means ± SD, n = 3). (**C**) Zeta-potential of ZIF-8, ZIF-8@BAN and PEG-FA@ZIF-8@BAN (means ± SD, n = 3).

presence of a hydration layer when the nanoparticles were dispersed in an aqueous solution. Figure 1C shows the zeta-potentials of ZIF-8, ZIF-8@BAN and PEG-FA@ZIF-8@BAN, with measurements of 25.47 ± 0.47 mV, −26.03 ± 0.58 mV, and −23.83 ± 1.1 mV, respectively. Due to the presence of a large number of phenolic hydroxyl groups on the surface of BAN, the zeta-potential turned negative after loading BAN, and remained negative after PEG-FA modification due to the presence of carboxyl groups in PEG-FA.

The crystal structures of each product were investigated by XRD. The XRD patterns of ZIF-8, ZIF-8@BAN, PEG-FA @ZIF-8@BAN and PEG-FA are shown in Figure 2A. The results showed that both blank ZIF-8 and drug-loaded ZIF-8 solids had a certain degree of crystallinity, and the XRD pattern data were more consistent with the reported crystal structure data of ZIF-8, which proved the successful synthesis of ZIF-8.[42] Rietveld analysis was performed on ZIF-8, ZIF-

8@BAN, and PEG-FA@ZIF-8@BAN using TOPAS software. As shown in Figure S2, the crystal structure of ZIF-8 after loading drugs and PEG-FA modification did not change much. However, the intensity of the diffraction peak of PEG-FA@ZIF-8@BAN at low angles was reduced after PEG-FA modification, which might be due to the existence of some masking effect on the crystal structure by the amorphous PEG-FA coating on the nanoparticle surface.

The UV spectra of ZIF-8, BAN, ZIF-8@BAN, and PEG-FA@ZIF-8@BAN were examined, and the absorption sites at the position of the 278 nm characteristic absorption peak of BAN were decreasing, indicating the successful encapsulation of BAN by PEG-FA@ZIF-8@BAN (Figure 2B). In addition, the modification process of the nanoplatform was further determined qualitatively by Fourier transform infrared (FT-IR) spectroscopy, as shown in Figure 2C, with the appearance of PEG-FA characteristic peaks at 3436 cm^{-1}
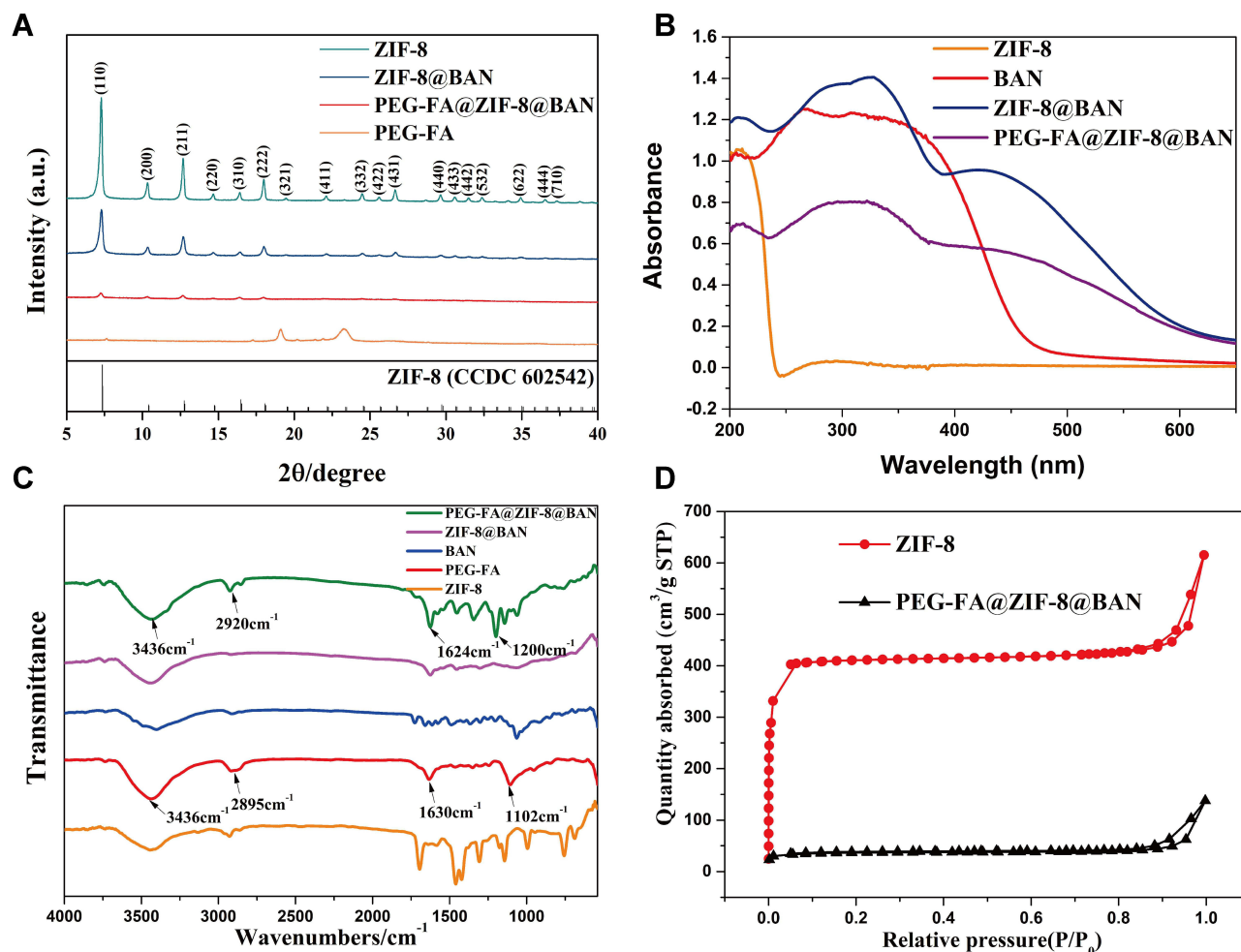

Figure 2 (**A**) XRD patterns of ZIF-8, ZIF-8@BAN, PEG-FA@ZIF-8@BAN and PEG-FA. (**B**) UV absorption patterns of ZIF-8, BAN, ZIF-8@BAN, and PEG-FA@ZIF-8@BAN. (**C**) FT-IR spectra of prepared ZIF-8, ZIF-8@BAN, PEG-FA@ZIF-8@BAN, BAN and PEG-FA. (**D**) N$_2$ absorption-desorption isotherms (h) of the prepared ZIF-8 and PEG-FA@ZIF-8@BAN.

(OH), 2920 cm^{-1} (-CH$_2$), 1624 cm^{-1} (C=O), and 1200 cm^{-1} (C-O-C) in the PEG-FA@ZIF-8@BAN spectrum, indicating the successful modification of PEG-FA. A comparison of the spectra of BAN and ZIF-8@BAN reveals that the characteristic peak of BAN at 1062 cm^{-1} does not appear in ZIF-8@BAN, indicating that the internal loading of ZIF-8 on BAN physically shields the characteristic peak. In addition, the imidazole ring of 2-methylimidazole has two double bonds and a lone pair of electrons from the nitrogen atom, which can interact in the plane of the imidazole ring. Thus, the imidazole ring can be considered as an aromatic compound and the BAN containing the benzene ring can also be loaded on ZIF-8 by π-π stacking.[43] In summary, BAN was successfully loaded in ZIF-8 and successfully modified PEG-FA on the surface to achieve the "targeting device" effect.

Brunel-Emmett-Teller (BET) measurements were performed to evaluate the porosity of PEG-FA@ZIF-8@BAN nanostructures, with ZIF-8 evaluated under similar conditions as a control variable. As shown in Figure 2D, they both exhibit typical type I N$_2$ absorption-desorption isotherms, which are one of the main features of microporous materials.[44] The BET surface area of ZIF-8 was 1267 m^2/g, while the surface area of PEG-FA@ZIF-8@BAN was reduced to 120 m^2/g. In addition, the corresponding pore volumes of the nanostructures of PEG-FA@ZIF-8@BAN were 0.85 cm^3/g and 0.21 cm^3/g, respectively. The pore size distribution results (Figure S3) shown that the pore width of ZIF-8 was mainly concentrated in micropores, and the pore width of PEG-FA@ZIF-8@BAN was concentrated in

mesopores (2–50 nm) or macropores. The possible reason was that the drug occupied the micropores resulting in the nitrogen gas being able to enter only into the mesopores or macropores. Therefore, the pore size of PEG-FA@ZIF-8@BAN measured by BET was larger than ZIF-8. The above results indicate the successful loading of BAN and the successful modification of PEG-FA.

In vitro Release of Drugs

In order to evaluate the loading and release behavior of ZIF-8 on BAN, we first established a standard curve of BAN solution with good linear relationship. It can be seen from Figure 3A that the absorbance of BAN at 278 nm shows an increasing trend with increasing concentration. As shown in Figure S4, the highest loading efficiency of ZIF-8@BAN was achieved when the mass ratio of ZIF-8 to BAN was 1:1. In addition, we repeatedly measured the loading efficiency of PEG-FA@ZIF-8@BAN and obtained the result of 41.45% ± 1.43%. We measured the entrapment efficiency of ZIF-8 for BAN as 65.83 ± 3.35%. Compared with other BAN nano-delivery systems, PEG-FA@ZIF-8@BAN has greater drug loading efficiency.[45,46]

In addition, we also measured the in vitro release behavior of PEG-FA@ZIF-8@BAN in PBS buffered solutions of different pH; as shown in Figure 3B, there was no significant release of the drug within 24 hours measured in neutral PBS solution, and the release amount was 11.03%, from which it can be inferred that PEG-FA@ZIF-8@BAN has good stability in a normal physiological environment. In contrast, the ZIF-8 metal-organic framework structure was broken
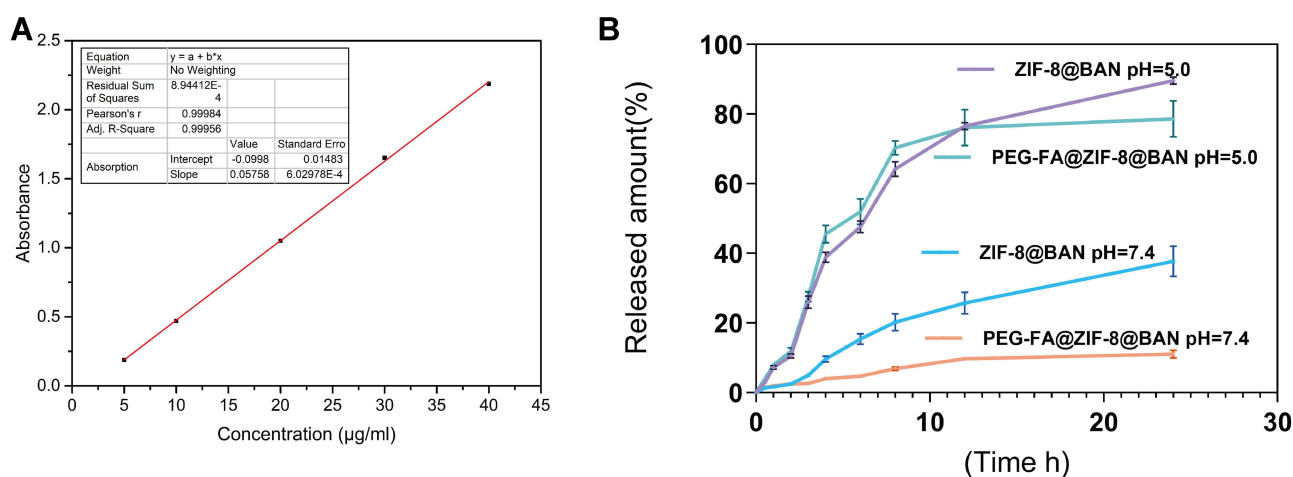

A

Equation	y = a + b*x	
Weight	No Weighting	
Residual Sum of Squares	8.94412E-4	
Pearson's r	0.99984	
Adj. R-Square	0.99956	
	Value	Standard Erro
Absorption Intercept	-0.0998	0.01483
Absorption Slope	0.05758	6.02978E-4

Figure 3 (**A**) Standard curve of BAN solution detected by UV spectrophotometer at 278 nm. (**B**) Release curves of BAN in PBS buffer solution at pH 5.0 or 7.4 (means ± SD, n = 3).

Table 1 Correlation Coefficients (R^2) and Release Exponent (n) According to the Korsmeyer-Peppas Model Used for Describing BAN Release Mechanisms

	ZIF-8@BAN		PEG-FA@ZIF-8@BAN	
	pH=5.0	pH=7.4	pH=5.0	pH=7.4
R^2	0.973	0.952	0.964	0.950
n	1.169	0.996	1.097	0.568

relatively quickly in the acidic environment and released the drug, with a final assay of up to 78.6% drug release. ZIF-8@BAN finally released 37.72% of the drug in a pH 7.4 environment. This may be due to the lack of protection of the PEG shell, which led to the cleavage of part of the metal-organic framework and the drug was released. The release of ZIF-8@BAN drug in an acidic environment finally reached 89.66%, indicating that the PEG-FA-modified nanoparticles have a better sustained-release effect. The Korsmeyer-Peppas model was used to fit the drug release curve. We found that the fitting results have a good linear relationship ($R^2 \geq 0.950$), indicating that the release of drugs under different pH environments conforms to the Korsmeyer-Peppas law. As shown in Table 1, the release constants (n) of ZIF-8@BAN in different pH environments were all greater than 0.89, indicating that the drug release mechanism of the nanosystem was mainly matrix erosion. The release mechanism of PEG-FA@ZIF-8@BAN at pH=5.0 was

mainly skeletal dissolution, while the drug release mechanism of PEG-FA@ZIF-8@BAN at pH = 7.4 included Ficks diffusion and erosion mechanisms (0.45 < n < 0.89).[47] PEG-FA modified ZIF-8@BAN nanoparticles do not cause drug leakage at normal physiological pH = 7.4. These results suggest that PEG-FA@ZIF-8 can serve as a good drug delivery platform for BAN.

FR Expression in MCF-7 Cells

The membrane surface of MCF-7 showed FR positive expression. Blue fluorescence represented the nucleus, while green fluorescence indicated FR on the MCF-7 cell membrane as pictured by the fluorochrome-conjugated (Alexa Fluor 488). The results are shown in Figure 4A. Green fluorescence was displayed on the corresponding cell membrane of each MCF-7 cell position. The results of this experiment shown that MCF-7 specifically expresses FR, and high expression of FR was expected to have more cellular uptake.

Cytotoxicity and Biocompatibility of Samples

The CCK-8 kit was used to detect the cytotoxicity of different concentrations of nanomaterials at different times of action. The cytotoxicity of the prepared PEG-FA@ZIF-8 blank material was firstly investigated. The
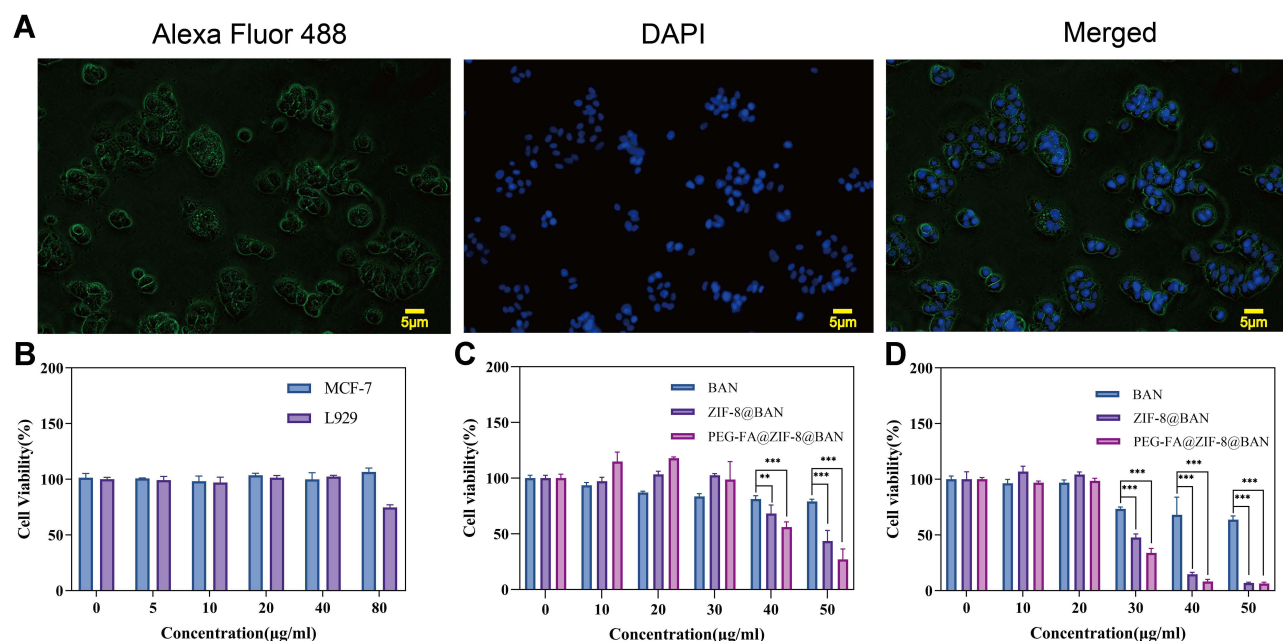

Figure 4 (**A**) MCF-7 cells for FR expression (scale bar: 5 μm). (**B**) Viability of MCF-7 cells and L929 cells after treatment with blank nanoparticles PEG-FA@ZIF-8 (means ± SD, n = 3). (**C**) Cell viability of MCF-7 cells after treatment with different samples containing the same BAN for 12 hours (means ± SD, n = 3). (**D**) Cell viability of MCF-7 cells after treatment with different samples containing the same BAN for 24 hours (means ± SD, n = 3). ** is $p < 0.01$, and ***is $p < 0.001$, compared with BAN group.
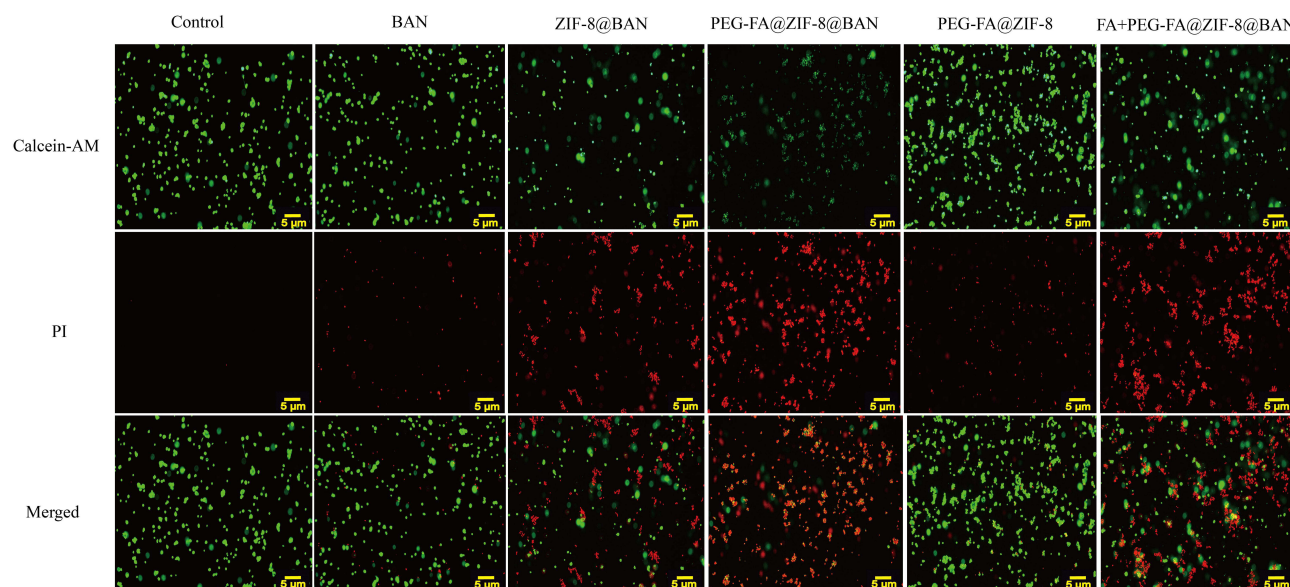
Control   BAN   ZIF-8@BAN   PEG-FA@ZIF-8@BAN   PEG-FA@ZIF-8   FA+PEG-FA@ZIF-8@BAN

Calcein-AM

PI

Merged

Figure 5 Fluorescence microscopy images using different samples treated with 40 μg/mL of BAN, all images on a scale of 5 μm.

results are shown in Figure 4B. The blank nanomaterial human breast cancer cells MCF-7 and normal mouse fibroblasts L929 did not show significant cytotoxicity in the dose range. Subsequently, as shown in Figure 4C and D, When MCF-7 cells were incubated with nanocomposites containing the same BAN concentration for different times, the cell survival showed a significant decreasing trend with increasing concentration, and the killing effect on tumor cells was stronger with increasing incubation time. The good tumor-killing effect of the nanoparticles was demonstrated by the cell survival rate of less than 10% after incubating MCF-7 cells with higher concentrations of ZIF-8@BAN and PEG-FA@ZIF-8@BAN for 24 hours.

Live and Dead Cell Staining

In addition to cytotoxicity assays, cell survival status was further observed by live/dead cell staining assays. As shown in Figure 5, no significant red fluorescence was found in the BAN and PEG-FA@ ZIF-8 groups, indicating no significant death of MCF-7 cells. In contrast, significant red fluorescence was found in ZIF-8@BAN and PEG-FA@ZIF-8@BAN, and the strongest red fluorescence was found in the PEG-FA @ZIF-8@BAN group, indicating massive death of cancer cells. Notably, when pre-incubated with PEG-FA, the killing effect on MCF-7 cells showed a significant decrease after the administration of

equal amounts of PEG-FA@ZIF-8@BAN, which was obviously due to the reduced therapeutic effect caused by the free folate blocking the folate receptors on the surface of the tumor cells so that PEG-FA@ZIF-8@BAN could not accumulate well in the tumor cells, showing the good tumor targeting of the material.

Cellular Uptake Experiments

Laser confocal microscopy was used to monitor the uptake process of the drug delivery system. As shown in Figure 6A-D, nucleic acid staining was performed using Hoechst 33342 to give a blue fluorescence and DCFH-DA reactive oxygen ROS fluorescent probe was used to detect intracellular reactive oxygen species production to give a green fluorescence. CLMS images showed that after incubation with nanoparticles for 0.5 hour, only a small amount of ROS was generated in the MCF-7 cells, showing a relatively faint green fluorescence. When the incubation time was increased to 3 hours, there was a large amount of ROS production and the green fluorescence intensity increased, indicating that a large number of nanoparticles were taken up by the cells.

When MCF-7 cells were treated with free PEG-FA preincubation for 2 hours and the PEG-FA@ZIF-8@BAN cell uptake experiments were performed again at different times, it was found that the green fluorescence
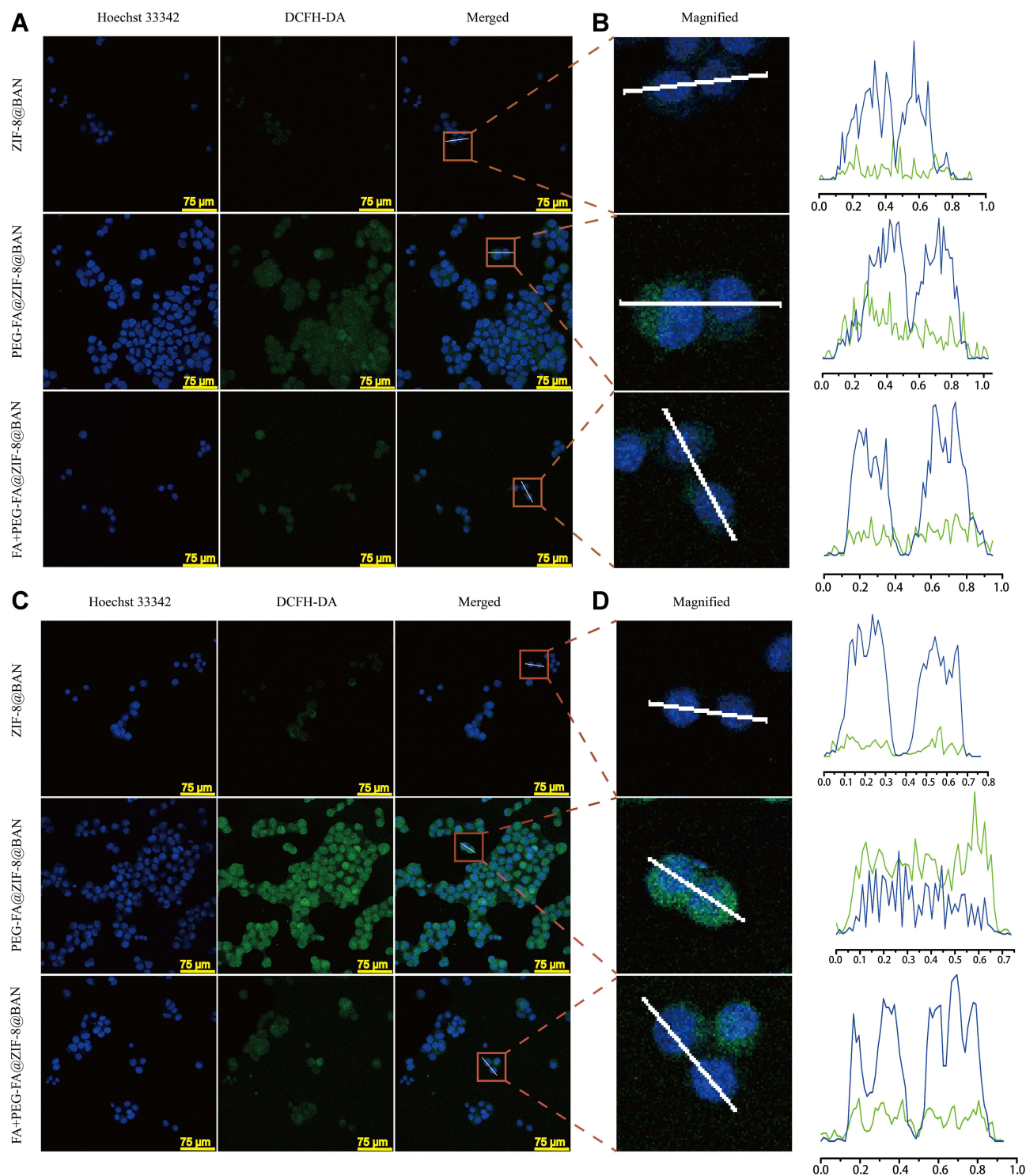
Figure 6 CLMS images of MCF-7 cells incubated with ZIF-8@BAN, PEG-FA@ZIF-8@BAN, and FA+ PEG-FA@ZIF-8@BAN in 0.5 hour and 3 hours. The scaling bars for all images are 75 μm. (**A** and **C**) are the images after merging of the corresponding images, and (**B** and **D**) are the magnified area images and the fluorescence intensity along the white line crossing.

produced in the cells was significantly weaker than in the group without the blocked receptor, which once again indicated that the cellular uptake of PEG-FA@ZIF-8@BAN was mediated by the folate receptor.[48]

Hemolytic Test

Blood compatibility is a vital factor for in vivo bio-applications when the materials are administered. Red blood cells (RBCs) hemolytic measurement is a simple
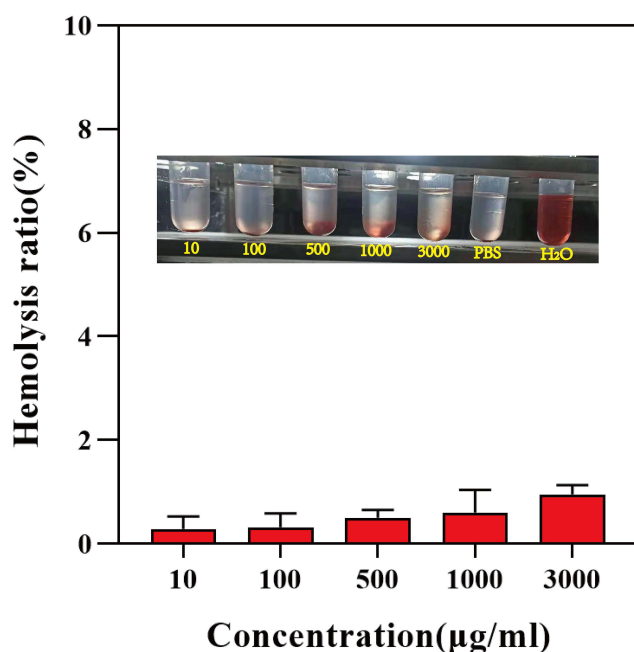
Figure 7 Hemolysis rate and images of different concentrations of PEG-FA@ZIF-8@BAN after co-incubation with erythrocyte suspension for 3 hours (means ± SD, n = 3).

and widely used method to research carrier-blood cells interaction.[49] Hemocompatibility was analyzed using 2% New Zealand White Rabbit Erythrocyte Suspension to ensure the biosafety of the PEG-FA @ZIF-8@BAN. Figure 7 demonstrates the hemolysis of different concentrations of material after coexistence with erythrocyte suspension for 3 hours. PBS and purified water were used as negative and positive controls, respectively. The results showed that PEG-FA @ZIF-8@BAN at all concentrations had no visible red color of red blood cells and its hemolysis ratio was less than 2%, indicating that PEG-FA@ZIF-8@BAN has a good safety profile.

In vivo Antitumor Research

After in vitro anti-tumor assays demonstrated the great potential of PEG-FA@ZIF-8@BAN to target tumors, in vivo level anti-tumor effects were examined by constructing a 4T1 tumor-bearing mouse model. Figure 8A shows a schematic diagram of the process of the in vivo anti-tumor assay. As shown in Figure 8B, there was no significant change in the body weight of each group during the treatment period, and the liver and kidney functions of each group

of mice as well as the normal mice were also tested by blood biochemical experiments (Figure S5), which showed that all the blood biochemical indices of the mice treated with PEG-FA@ZIF-8@BAN were normal, indicating the safety and non-toxicity of PEG-FA@ZIF-8@BAN as an anti-tumor treatment system. As shown by the changes of tumor volume in each group of mice (Figure 8C), tumor growth was very rapid in the PBS and BAN groups, and ZIF-8@BAN exhibited some tumor suppressive effect, however, PEG-FA@ZIF-8@BAN showed a better suppressive effect with very slow tumor growth. In addition, the tumors were photographed as well as weighed after the treatment, as shown in Figure 8D and E, and it was found that both ZIF-8@BAN and PEG-FA@ZIF-8@BAN had the effect of reducing tumor weight, and the PEG-FA@ZIF-8@BAN group had the stronger inhibitory effect. Because of the targeting effect of folic acid, PEG-FA@ZIF-8@BAN severely inhibited the proliferation of tumors.[50] The findings again suggest that PEG-FA@ZIF-8@BAN can serve as a good nano-targeting platform for tumor treatment in vivo. Meanwhile, the results of dUTP-bioprotein end-labeling assay staining using hematoxylin and eosin (H&E) and terminal deoxynucleotidyl transferase-mediated staining (Figures 9 and 10) showed cell shrinkage and nuclear loss in tumor cells under ZIF-8@BAN and PEG-FA@ZIF-8@BAN treatment, and more severe apoptosis in tumor cells, showing a killing effect on tumor tissue. Compared with the control group, no significant cell damage or apoptosis was observed in the major organ cells of each treatment group, indicating that there was no significant toxicity to the major organs in each treatment group.

Conclusion

In conclusion, we constructed a folate receptor responsive BAN nano-delivery system to improve the therapeutic effect of BAN on breast cancer. The synthesis of PEG-FA@ZIF-8@BAN was simple and under mild conditions, making its mass production possible. This drug delivery system has high loading efficiency and can release large amounts of drug and zinc ions in the micro-acidic environment of tumors, while the release rate is 11.03% under normal physiological conditions, and intravenous injection can achieve folate receptor release
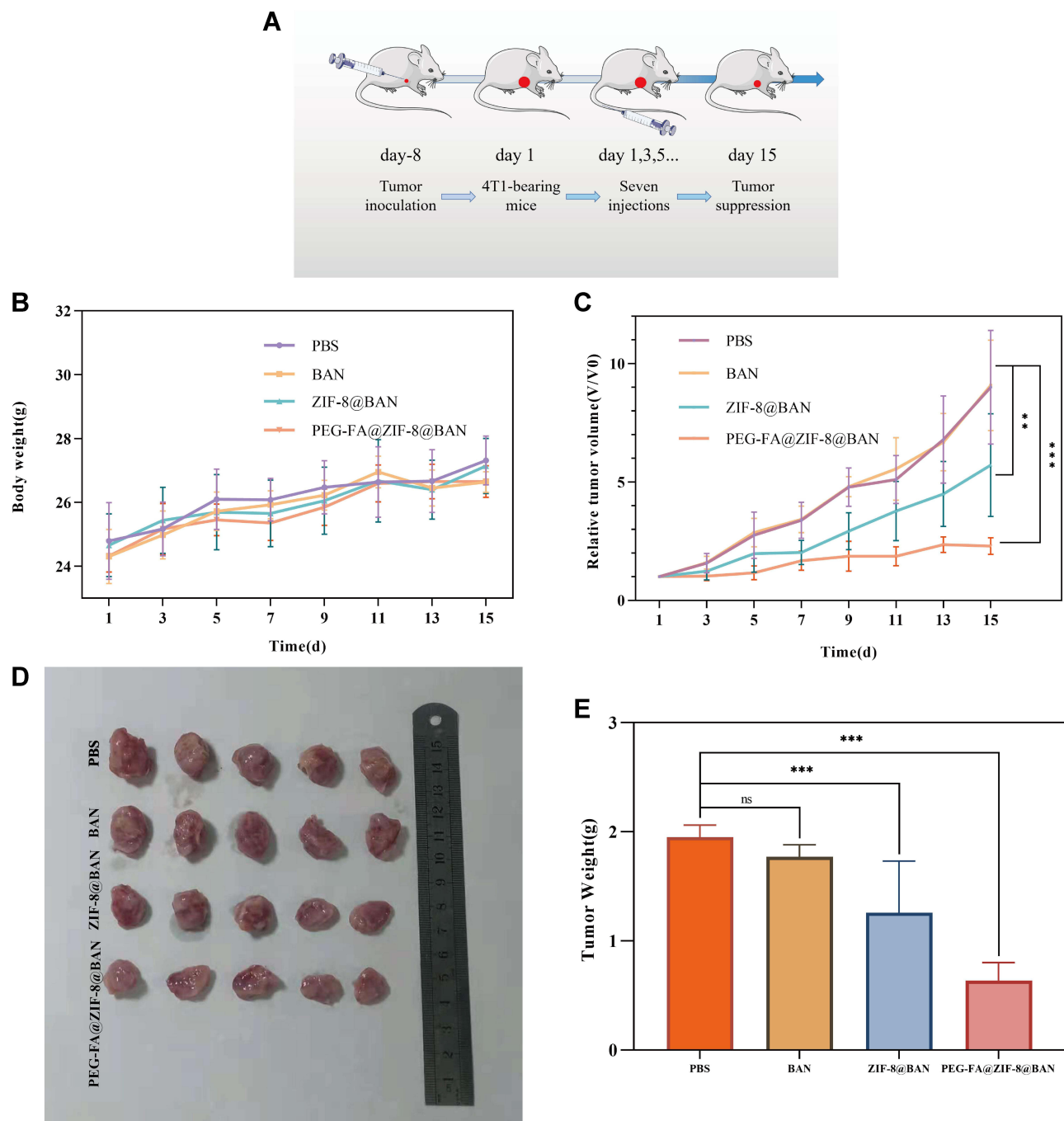
Figure 8 (**A**) Schematic diagram of in vivo antitumor treatment. (**B**) Changes in body weight during treatment (means ± SD, n = 7). (**C**) Relative tumor volume (means ± SD, n = 7). (**D**) Representative pictures of the final dissected tumor. (**E**) Tumor weight (means ± SD, n = 7). $^{ns}p > 0.05$, $^{**}p < 0.01$, $^{***}p < 0.001$, compared with PBS group.

properties. In vitro cytotoxicity as well as live/dead cell staining studies of PEG-FA@ZIF-8@BAN exhibited significant tumor cell killing effects compared to the prodrug, but the carrier material showed good biocompatibility. Cellular uptake assays demonstrated that the folate receptor-mediated drug delivery system could accumulate in tumor cells. In addition, in vivo experiments showed that PEG-FA@ZIF-8@BAN significantly inhibited tumor growth in 4T1 tumor-bearing mice. The above results suggest that PEG-FA@ZIF-8@BAN may be an effective treatment for breast cancer.
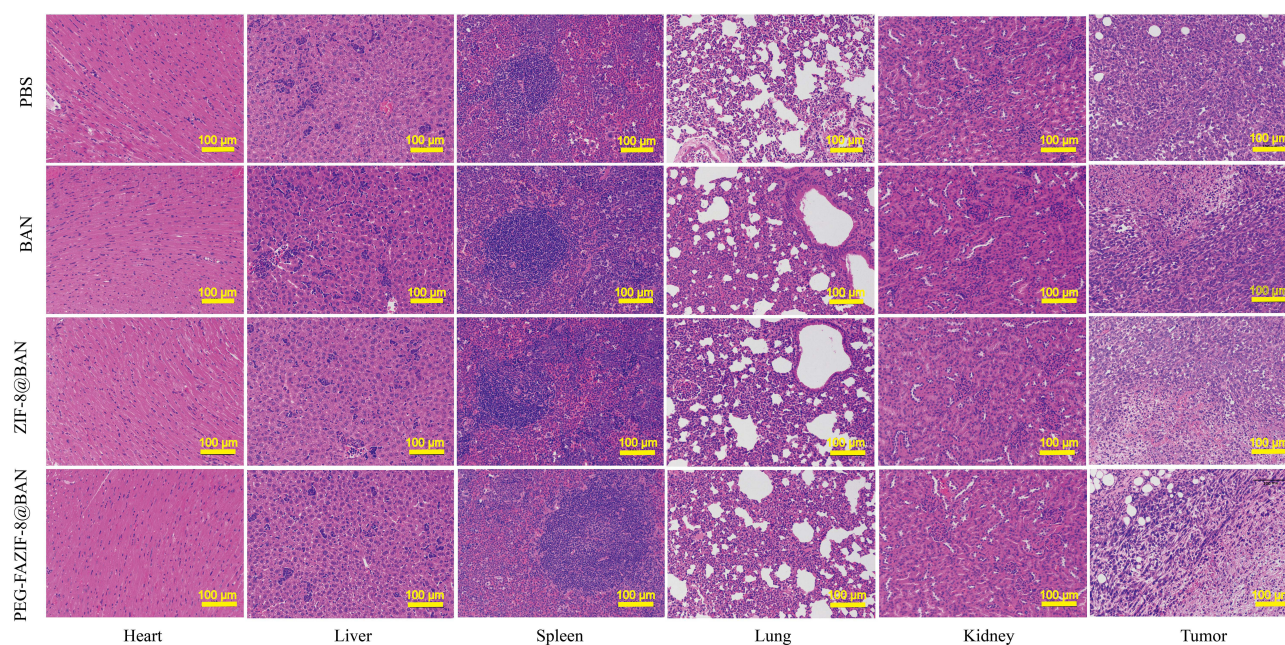
Figure 9 H&E staining of major organs (heart, liver, spleen, lung, kidney) and tumor tissues of treated mice (scale bar: 100 μm).
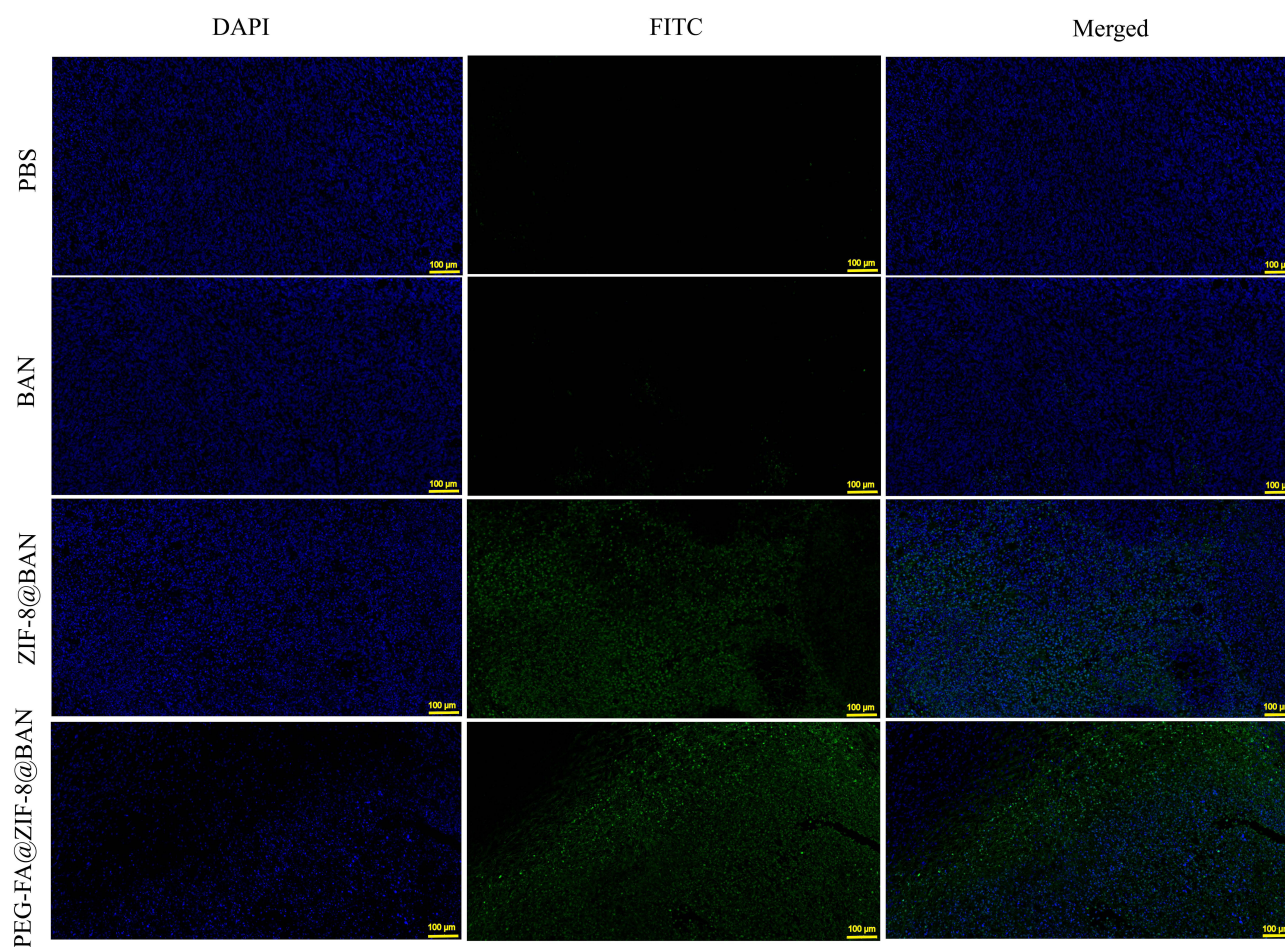

Figure 10 TUNEL stained images of tumor tissue in treated mice (scale bar: 100 μm).

Acknowledgments

Funding

Disclosure

The authors report no conflicts of interest in this work.

References

1. Fisusi FA, Akala EO. Drug combinations in breast cancer therapy. *Pharm Nanotechnol.* 2019;7(1):3–23. doi:10.2174/2211738 507666190122111224

2. Semin JN, Palm D, Smith LM, Ruttle S. Understanding breast cancer survivors' financial burden and distress after financial assistance. *Support Care Cancer.* 2020;28(9):4241–4248. doi:10.1007/s00520-019-05271-5

3. Fitzmaurice C, Abate D, Abbasi N, et al. Global, regional, and national cancer incidence, mortality, years of life lost, years lived with disability, and disability-adjusted life-years for 29 cancer groups, 1990 to 2017: a systematic analysis for the global burden of disease study. *JAMA Oncol.* 2019;5(12):1749–1768. doi:10.1001/jamaoncol.2019.2996

4. Yu T, Li Y, Gu X, Li Q. Development of a hyaluronic acid-based nanocarrier incorporating doxorubicin and cisplatin as a pH-Sensitive and CD44-targeted anti-breast cancer drug delivery system. *Front Pharmacol.* 2020;11:532457. doi:10.3389/fphar.2020.532457

5. Cheng L, Wang C, Feng L, Yang K, Liu Z. Functional nanomaterials for phototherapies of cancer. *Chem Rev.* 2014;114(21):10869–10939. doi:10.1021/cr400532z

6. Cheng CS, Chen J, Tan HY, Wang N, Chen Z, Feng Y. Scutellaria baicalensis and cancer treatment: recent progress and perspectives in biomedical and clinical studies. *Am J Chin Med.* 2018;46(1):25–54.

7. Song JW, Long JY, Xie L, et al. Applications, phytochemistry, pharmacological effects, pharmacokinetics, toxicity of Scutellaria baicalensis Georgi. and its probably potential therapeutic effects on COVID-19: a review. *Chin Med.* 2020;15(1):102. doi:10.1186/s13020-020-00384-0

8. Tao Y, Zhan S, Wang Y, et al. Baicalin, the major component of traditional Chinese medicine Scutellaria baicalensis induces colon cancer cell apoptosis through inhibition of oncomiRNAs. *Sci Rep.* 2018;8(1):14477. doi:10.1038/s41598-018-32734-2

9. Wang Z, Ma L, Su M, et al. Baicalin induces cellular senescence in human colon cancer cells via upregulation of DEPP and the activation of Ras/Raf/MEK/ERK signaling. *Cell Death Dis.* 2018;9(2):217. doi:10.1038/s41419-017-0223-0

10. Yu Y, Pei M, Li L. Baicalin induces apoptosis in hepatic cancer cells in vitro and suppresses tumor growth in vivo. *Int J Clin Exp Med.* 2015;8(6):8958–8967.

11. Lin C, Tsai SC, Tseng MT, et al. AKT serine/threonine protein kinase modulates baicalin-triggered autophagy in human bladder cancer T24 cells. *Int J Oncol.* 2013;42(3):993–1000. doi:10.3892/ijo.2013.1791

12. Zhu Y, Fang J, Wang H, et al. Baicalin suppresses proliferation, migration, and invasion in human glioblastoma cells via Ca $(^{2+})$--dependent pathway. *Drug Des Devel Ther.* 2018;12:3247–3261. doi:10.2147/DDDT.S176403

13. Gong WY, Zhao ZX, Liu BJ, Lu LW, Dong JC. Exploring the chemopreventive properties and perspectives of baicalin and its aglycone baicalein in solid tumors. *Eur J Med Chem.* 2017;126:844–852. doi:10.1016/j.ejmech.2016.11.058

14. Li-Weber M. New therapeutic aspects of flavones: the anticancer properties of Scutellaria and its main active constituents Wogonin, Baicalein and Baicalin. *Cancer Treat Rev.* 2009;35(1):57–68. doi:10.1016/j.ctrv.2008.09.005

15. Lan M, Kong Z, Liu F, et al. Activating Caspase-8/Bid/ROS signaling to promote apoptosis of breast cancer cells by folate-modified albumin baicalin-loaded nanoparticles. *Nanotechnology.* 2021. doi:10.1088/1361-6528/ac197b

16. Zhang, Huang, Li, et al. Baicalin induces apoptosis and inhibits migration/invasion of breast cancer cell MDA-MB-231 through reactive oxygen species-mediated activation of p38/c-Jun N-terminal kinase signaling pathway. *J Biomater Tiss Eng.* 2018;8 (7):1022–1030. doi:10.1166/jbt.2018.1838

17. Wang N, Tang LJ, Zhu GQ, et al. Apoptosis induced by baicalin involving up-regulation of P53 and bax in MCF-7 cells. *J Asian Nat Prod Res.* 2008;10(11–12):1129–1135. doi:10.1080/10286020802410664

18. Wu H, Long X, Yuan F, et al. Combined use of phospholipid complexes and self-emulsifying microemulsions for improving the oral absorption of a BCS class IV compound, baicalin. *Acta Pharm Sin B.* 2014;4(3):217–226. doi:10.1016/j.apsb.2014.03.002

19. Zhao L, Wei Y, Huang Y, He B, Zhou Y, Fu J. Nanoemulsion improves the oral bioavailability of baicalin in rats: in vitro and in vivo evaluation. *Int J Nanomedicine.* 2013;8:3769–3779. doi:10.2147/IJN.S51578

20. Dong K, Zhang Y, Zhang L, Wang Z, Ren J, Qu X. Facile preparation of metal-organic frameworks-based hydrophobic anticancer drug delivery nanoplatform for targeted and enhanced cancer treatment. *Talanta.* 2019;194:703–708. doi:10.1016/j.talanta.2018.10.101

21. Horcajada P, Gref R, Baati T, et al. Metal-organic frameworks in biomedicine. *Chem Rev.* 2012;112(2):1232–1268. doi:10.1021/cr200256v

22. Gao L, Chen Q, Gong T, Liu J, Li C. Recent advancement of imidazolate framework (ZIF-8) based nanoformulations for synergistic tumor therapy. *Nanoscale.* 2019;11(44):21030–21045. doi:10.1039/C9NR06558J

23. Sun Y, Zheng L, Yang Y, et al. Metal-organic framework nanocarriers for drug delivery in biomedical applications. *Nanomicro Lett.* 2020;12(1):103. doi:10.1007/s40820-020-00423-3

24. Chen X, Tong R, Shi Z, et al. MOF nanoparticles with encapsulated autophagy inhibitor in controlled drug delivery system for antitumor. *ACS Appl Mater Interfaces.* 2018;10(3):2328–2337. doi:10.1021/acsami.7b16522

25. Chen WH, Luo GF, Vázquez-González M, et al. Glucose-responsive metal-organic-framework nanoparticles act as "smart" sense-and-treat carriers. *ACS Nano.* 2018;12(8):7538–7545. doi:10.1021/acsnano.8b03417

26. Liang Z, Yang Z, Yuan H, et al. A protein@metal-organic framework nanocomposite for pH-triggered anticancer drug delivery. *Dalton Trans.* 2018;47(30):10223–10228. doi:10.1039/C8DT01789A

27. Narmani A, Rezvani M, Farhood B, et al. Folic acid functionalized nanoparticles as pharmaceutical carriers in drug delivery systems. *Drug Dev Res.* 2019;80(4):404–424. doi:10.1002/ddr.21545

28. Watanabe K, Kaneko M, Maitani Y. Functional coating of liposomes using a folate- polymer conjugate to target folate receptors. *Int J Nanomedicine.* 2012;7:3679–3688. doi:10.2147/IJN.S32853

29. Zhong S, Zhang H, Liu Y, et al. Folic acid functionalized reduction-responsive magnetic chitosan nanocapsules for targeted delivery and triggered release of drugs. *Carbohydr Polym.* 2017;168:282–289. doi:10.1016/j.carbpol.2017.03.083

30. Yoo HS, Park TG. Folate-receptor-targeted delivery of doxorubicin nano-aggregates stabilized by doxorubicin-PEG-folate conjugate. *J Control Release*. 2004;100(2):247–256. doi:10.1016/j.jconrel.2004.08.017

31. El-Hammadi MM, Delgado ÁV, Melguizo C, Prados JC, Arias JL. Folic acid-decorated and PEGylated PLGA nanoparticles for improving the antitumour activity of 5-fluorouracil. *Int J Pharm*. 2017;516(1–2):61–70. doi:10.1016/j.ijpharm.2016.11.012

32. Ma K, Li W, Zhu G, et al. PEGylated DOX-coated nano graphene oxide as pH-responsive multifunctional nanocarrier for targeted drug delivery. *J Drug Target*. 2021;29(8):884–891. doi:10.1080/1061186X.2021.1887200

33. Zhou Y, Chen R, Yang H, et al. Light-responsive polymersomes with a charge-switch for targeted drug delivery. *J Mater Chem B*. 2020;8(4):727–735. doi:10.1039/C9TB02411E

34. Wang M, Long J, Zhang S, et al. Folate-targeted anticancer drug delivery via a combination strategy of a micelle complex and reducible conjugation. *ACS Biomater Sci Eng*. 2020;6(3):1565–1572. doi:10.1021/acsbiomaterials.9b01920

35. Alibolandi M, Abnous K, Sadeghi F, Hosseinkhani H, Ramezani M, Hadizadeh F. Folate receptor-targeted multimodal polymersomes for delivery of quantum dots and doxorubicin to breast adenocarcinoma: in vitro and in vivo evaluation. *Int J Pharm*. 2016;500(1–2):162–178. doi:10.1016/j.ijpharm.2016.01.040

36. Borah PK, Das AS, Mukhopadhyay R, Sarkar A, Duary RK. Macromolecular design of folic acid functionalized amylopectin-albumin core-shell nanogels for improved physiological stability and colon cancer cell targeted delivery of curcumin. *J Colloid Interface Sci*. 2020;580:561–572. doi:10.1016/j.jcis.2020.07.056

37. Koirala N, Das D, Fayazzadeh E, et al. Folic acid conjugated polymeric drug delivery vehicle for targeted cancer detection in hepatocellular carcinoma. *J Biomed Mater Res A*. 2019;107(11):2522–2535. doi:10.1002/jbm.a.36758

38. Ahmed A, Karami A, Sabouni R, Husseini GA, Paul V. pH and ultrasound dual-responsive drug delivery system based on PEG–folate-functionalized iron-based metal–organic framework for targeted doxorubicin delivery. *Colloid Surface A*. 2021;626:127062. doi:10.1016/j.colsurfa.2021.127062

39. Heidari Majd M, Barar J, Asgari D, et al. Targeted fluoromagnetic nanoparticles for imaging of breast cancer mcf-7 cells. *Adv Pharm Bull*. 2013;3(1):189–195. doi:10.5681/apb.2013.031

40. Yan H, You Y, Li X, et al. Preparation of RGD peptide/folate acid double-targeted mesoporous silica nanoparticles and its application in human breast cancer MCF-7 cells. *Front Pharmacol*. 2020;11:898. doi:10.3389/fphar.2020.00898

41. Zagami R, Rapozzi V, Piperno A, et al. Folate-decorated amphiphilic cyclodextrins as cell-targeted nanophototherapeutics. *Biomacromolecules*. 2019;20(7):2530–2544. doi:10.1021/acs.biomac.9b00306

42. Shi Z, Chen X, Zhang L, et al. FA-PEG decorated MOF nanoparticles as a targeted drug delivery system for controlled release of an autophagy inhibitor. *Biomater Sci*. 2018;6(10):2582–2590. doi:10.1039/C8BM00625C

43. Jiang W, Zhang H, Wu J, et al. CuS@MOF-based well-designed quercetin delivery system for chemo-photothermal therapy. *ACS Appl Mater Interfaces*. 2018;10(40):34513–34523. doi:10.1021/acsami.8b13487

44. Sun Q, Bi H, Wang Z, et al. Hyaluronic acid-targeted and pH-responsive drug delivery system based on metal-organic frameworks for efficient antitumor therapy. *Biomaterials*. 2019;223:119473. doi:10.1016/j.biomaterials.2019.119473

45. Chen Y, Minh LV, Liu J, et al. Baicalin loaded in folate-PEG modified liposomes for enhanced stability and tumor targeting. *Colloids Surf B Biointerfaces*. 2016;140:74–82. doi:10.1016/j.colsurfb.2015.11.018

46. Meng F, Liu F, Lan M, Zou T, Cai Y. Preparation and evaluation of folate-modified albumin baicalin-loaded nanoparticles for the targeted treatment of breast cancer. *J Drug Deliv Sci Tec*. 2021;65:102603. doi:10.1016/j.jddst.2021.102603

47. Peng H, Xiong H, Li J, et al. Vanillin cross-linked chitosan microspheres for controlled release of resveratrol. *Food Chem*. 2010;121(1):23–28. doi:10.1016/j.foodchem.2009.11.085

48. Kunjiappan S, Govindaraj S, Parasuraman P, et al. Design, in silico modelling and functionality theory of folate-receptor-targeted myricetin-loaded bovine serum albumin nanoparticle formulation for cancer treatment. *Nanotechnology*. 2020;31(15):155102. doi:10.1088/1361-6528/ab5c56

49. Ma N, Zhang B, Liu J, Zhang P, Li Z, Luan Y. Green fabricated reduced graphene oxide: evaluation of its application as nano-carrier for pH-sensitive drug delivery. *Int J Pharm*. 2015;496(2):984–992. doi:10.1016/j.ijpharm.2015.10.081

50. Ma Z, Pi J, Zhang Y, et al. Enhanced anticancer efficacy of dual drug-loaded self-assembled nanostructured lipid carriers mediated by pH-responsive folic acid and human-derived cell penetrating peptide dNP2. *Pharmaceutics*. 2021;13:5. doi:10.3390/pharmaceutics13050600